A Numerical Simulation of Fog Dissipation Using Passive Burner Lines. Part I: Model Development and Comparison with Observations

PAUL M. TAG

Naval Environmental Prediction Research Facility, Monterey, CA 93940

(Manuscript received 13 February 1979, in final form 4 August 1979)

ABSTRACT

A two-dimensional model is developed to simulate dissipation of fog using passive burner lines under either cross-wind or no-wind conditions. The vorticity model developed by Murray (1970) forms the basis for the development. Among the additions to the model are a stretched vertical grid, provision for an ambient wind field and variable eddy exchange coefficients.

The model is tested by comparing results to empirical temperature distribution data resulting from burner lines, located both outdoors and in a wind tunnel, positioned in a cross wind. Equally good comparisons are achieved by running the model at these two different physical scales. It is determined that the parameterization of the eddy coefficients most influences the resulting temperature profiles, and that a form in which deformation and buoyancy are summed gives the best results. A coefficient based solely on the deformation or vorticity gradients is found to be inadequate. Several additional experiments which utilize a soil heat flux parameterization support empirical estimates of a 5% heat loss to the soil.

1. Introduction

Of the several techniques which have been proposed for dissipating warm fog, the use of heat is the only operationally proven technique. In 1970, an underground system of jet engines was installed for operational use in fog dissipation at Orly Airport in Paris.[1] Together with a second installation at Charles de Gaulle Airport, 126 visibility-enhanced landings, which represented more than 10 000 passengers carried, were made during the winter of 1975–76. In 1972, the U.S. Air force initiated a pilot study using passive burner lines (as opposed to momentum heat sources) at Vandenburg Air Force Base, California (Kunkel *et al.*, 1974). In 1973, consideration was given to development of a passive ground-based system for Travis Air Force Base, California[2]; parallel burner lines, as used in the World War II FIDO system (see Rankine, 1950), were proposed for both sides of an instrumented runway. The concept of using passive burner lines alone was later abandoned by the Air Force in favor of a momentum-augmented heat system (Kunkel, 1979).

The objective of this study is to develop and use a two-dimensional model to simulate dissipation of fog using passive burner lines. Part I discusses model development, comparison with data, and refinement of the model to best simulate this data. Part II discusses sensitivity experiments that bracket the range of environmental conditions of interest in an operational environment.

2. Model development

a. Objectives and requirements

The general objective of the numerical simulations is to predict the evolution and final steady-state temperature structure over and downwind from one or more burner lines positioned on the ground. This objective follows directly from a conceptual analysis of whether the use of heat can be an effective technique for improving the visibility over an airport runway or any other surface. This analysis relates to two questions: first, can a minimal rise in air temperature cause a substantial improvement in visibility (and within a reasonable time frame); and second, can such a temperature rise be distributed into a sufficiently large, or correctly located, volume so as to be useful?

In order to determine the degree of temperature rise which is necessary to evaporate fog droplets, and thus improve visibility, numerical calculations were performed with a microphysical model which predicts the growth and evaporation of a size spectrum of fog droplets. Fig. 1 depicts results from an

[1] Fabre, R., 1971: Aeroport D'Orly—Installation De Denubulation Turboclair. Report by the Aeroport de Paris and Société Bertin et Cie, 39 pp.

[2] Weinstein, A. I., 1973: Thermal warm fog dissipation—heat requirements and projected utilization of a system for Travis AFB, California. *Air Force Surv. Geophys.* No. 270, AFCRL-TR-73-0367, 22 pp. [DDC or NTIS AD-766 247.]

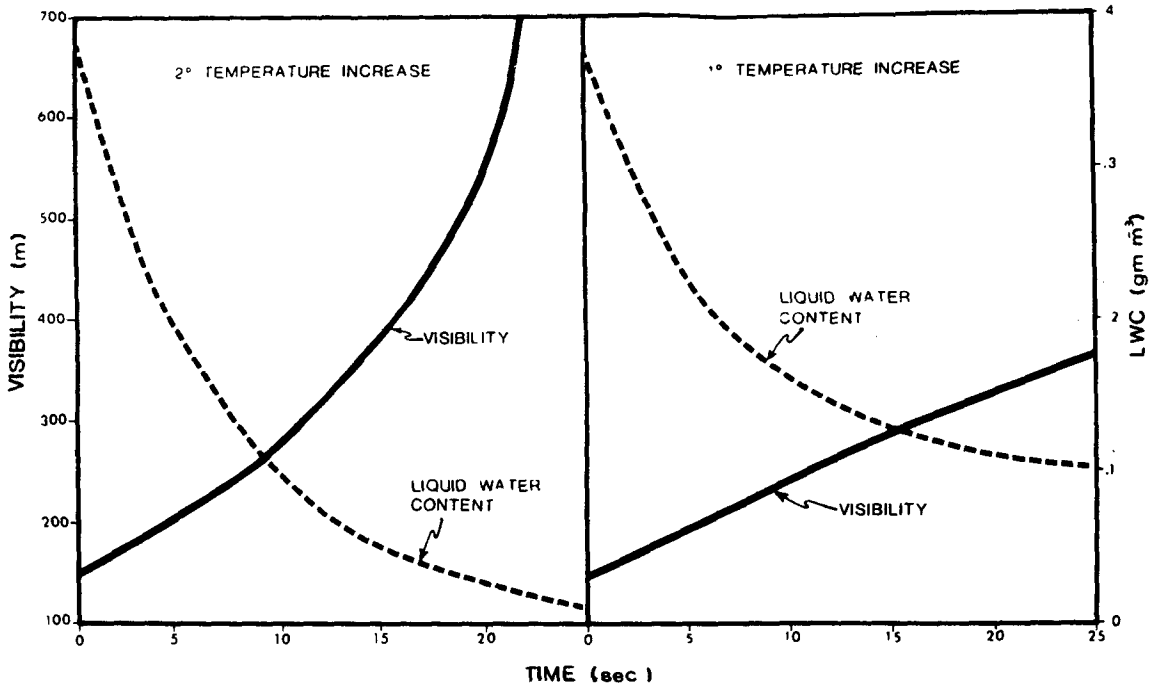

FIG. 1. Visibility and LWC change in response to an instantaneous temperature rise.

experiment simulating a moderately dense, maritime fog which has droplets ranging from 3 to 20 μm in radius and a liquid water content (LWC) of 0.39 g m^{-3}, and produces a calculated initial visibility of 143 m. Visibility and LWC are plotted as a function of time for a 1 and 2°C instantaneous temperature rise. The increase in visibility, accompanied by a decrease in LWC, is quite dramatic for the 2°C increase, and slightly less so for the 1°C temperature change. More important is the time frame within which the change occurs—on the order of 30 s. This time frame must be compared to those of chemical dessicants, which are of the order of 20–30 min (see, e.g., Tag, 1977).

This numerical simulation clearly indicates that the above second question poses the only obstacle to a successful heat-based fog dispersal system. Consequently, the primary objective of the model to be developed will be to predict the low-level thermal structure resulting from heat generated by a burner line.

To accomplish this objective, the model must meet certain minimum requirements. First, at least two space dimensions are required. Second, because simulated burner lines will result in strong gradients near the lower boundary, the model must have adequate resolution there. And third, because improved visibility in fog is the eventual goal of the heating, the evaporation of fog liquid water must be included and linked directly to the thermal structure in the model domain.

b. *Outline of the basic model*

Two of the above requirements are met in the vorticity model developed by Murray (Murray, 1970; Murray and Koenig, 1972); it is two-dimensional and based on the Boussinesq approximation. Such an approximation is acceptable because of the shallow domain appropriate here. The model was designed to be used in either the axial or the slab-symmetric mode. The latter is quite appropriate here for the simulation of a long burner line. In addition, parameterization of condensation and evaporation is an inherent part of the Murray model, with water being partitioned into vapor and suspended cloud liquid.

c. *Grid stretching*

To permit adequate resolution near the surface, but yet remove far enough the top boundary of the model domain, a stretched grid was implemented in the vertical. The coordinate transformation approach was chosen over an expanded mesh scheme because of its smaller truncation error (Roach, 1972). This transformation is effected by changing the vertical coordinate z to another variable s, using a form based on the hyperbolic tangent

$$s\left(\frac{z}{z_{\max}}\right) = \frac{\alpha \dfrac{z}{z_{\max}} + \tanh\left(\dfrac{z}{\sigma z_{\max}}\right)}{\alpha + \tanh(1/\sigma)} \qquad (1)$$

in which z_{max} is the value of z at the upper boundary. Sigma and alpha control the degree of stretching. The choice of these parameters and the resulting vertical extent of the domain will be discussed later.

d. Ambient wind simulation

Because many of the experiments of interest involve an ambient wind perpendicular to the burner line, this option was developed for the model. A crosswind in u, constant with height, was adopted for the crosswind experiments.

Since $u = -\partial\psi/\partial z$, the assumption of a reference state with a constant horizontal wind of $\bar{u}$ and no vertical wind leads to

$$\int_{\bar{\psi}_B}^{\bar{\psi}} d\bar{\psi} = -\bar{u} \int_0^z dz$$

or

$$\bar{\psi}(z) = \bar{\psi}_B - \bar{u}z. \tag{2}$$

If $\bar{\psi}(0)$ is arbitrarily assigned the value zero, this prescription defines the flow everywhere in the reference state (i.e., at initial time) and also gives the Dirichlet boundary conditions for the Poisson equation $\nabla^2\psi = -\eta$ that must be solved to determine the flow at later times. Since $\eta = \partial u/\partial z - \partial w/\partial x$, the vorticity must vanish in the reference state:

$$\bar{\eta} = \frac{\partial \bar{u}}{\partial z} = 0.$$

e. Boundary conditions

Following Murray and Koenig (1972), the upper and lower horizontal surfaces are considered to be rigid and free-slipping ($\partial u/\partial z = 0$ at $z = 0, z_{max}$). For the lateral boundaries, two sets of boundary conditions were assigned to the dynamic parameters. This option allows for optimization of the available model domain and also simplifies simulation of the two intended field situations. For the no-wind (hereafter referred to as NOW) simulations, the lateral boundaries are assumed to be rigid and free-slipping. The use of these "reflective" conditions for NOW cases is very desirable because it effectively permits the model domain to be doubled. Because two burner lines, one on either side of the airport runway, are necessary if there is no cross wind, the reflective boundary which is centered on the simulated runway is ideal. Although a reflective outer boundary is unnecessary, it will be far enough removed from the principal circulations to have little effect.

For the cross-wind (hereafter referred to as CRW) simulations, the ambient wind is held constant at both the upwind and downwind boundary. Assuming that $\partial w/\partial x = 0$ at the boundaries, η is equal to zero if u remains constant with height. Maintenance of a zero value for η at the lateral boundaries, and a specilfied ψ at the upper and lower boundaries, assures a constant ambient flow as inflow to, and outflow from, the model domain. It is assumed that the direction of flow at these boundaries never reverses.

Separate lateral boundary conditions are required for the thermodynamic variables. For the NOW simulations, where reflective boundaries are imposed, no additional requirements are necessary. Specification of $u = 0$ precludes flow across these surfaces.

For CRW simulations, the lateral boundaries will be viewed as "flow through" surfaces. The upwind boundary, representing unmodified ambient air, is handled simply by allowing parameters there to remain unchanged during the course of the run. At the downwind, right-hand boundary (R) we will assume that the second derivative is equal to that defined at R − 1. This specification again presumes that flow is always outward and never reverses. Utilizing centered space differences, it can be easily shown that

$$N_{R+1} = N_{R-2} + 3N_R - 3N_{R-1},$$

where N is any thermodynamic parameter. Several exploratory experiments in which the thermodynamic perturbations were permitted to flow completely through the downwind boundary indicated this boundary condition to be satisfactory. In practice, the domain is made sufficiently wide to preclude significant perturbations reaching this surface.

f. Solution of Poisson's equation

The successive overrelaxation technique used by Murray for solving Poisson's equation $\nabla^2\psi = -\eta$ was replaced by a direct solution type using a "block cyclic reduction" technique first introduced by Buneman.[3] This technique was programmed by Roland Sweet of the National Center for Atmospheric Research and modified for the stretched grid by Rosmond.[4] Rosmond and Faulkner (1976) describe this "direct solver." For a square grid of 65 points, the direct solver is approximately 35 times faster than successive overrelaxation (the method used in previous versions of the model), and solutions are correct to machine accuracy.

g. Heat and moisture input

Because the purpose of the model is to simulate the movement of heat from a line source, provision must be made for including relevant source terms. Sensible heat can be added simply by including an

[3] Buneman, O., 1969: A compact noniterative Poisson solver. SUIPR Rep. No. 294, Institute for Plasma Research, Stanford University, Palo Alto, CA, 9 pp. [NTIS SU-IPR-294.]

[4] Rosmond, T. E., 1975: Subroutines for direct solution of two-dimensional elliptic equations. Environmental Prediction Research Facility, Monterey, CA, Comp. Prog. Note 23, 32 pp. [DDC or NTIS ADA-013-190.]

additional source term, S_H[K s^{-1}], in the differential equation for perturbation temperature

$$S_H = \frac{Q_H}{V\rho_d(C_p + q_v C_{pv} + q_f C_w)}, \quad (3)$$

where Q_H is the rate of sensible heat addition (J s^{-1}), V the volume of air to which Q_H is added, ρ_d the mean dry air density, q_v and q_f the mixing ratios of water vapor and fog, and C_p, C_{pv} and C_w the respective specific heats for dry air, water vapor and water.

Because water vapor is a by-product of hydrocarbon combustion, an additional source term, S_v[s^{-1}], is required in the water vapor equation

$$S_v = \frac{1}{\rho_d}\frac{\partial \rho_v}{\partial t}, \quad (4)$$

where

$$\frac{\partial \rho_v}{\partial t} = \frac{\gamma S_f}{V} \quad (5)$$

and ρ_v is the density of water vapor, γ the mass of water vapor produced during the combustion of unit mass of fuel, and S_f the fuel consumption rate ($kg\ s^{-1}$). Because our model is two-dimensional, both S_H and S_f above are defined per length of y direction distance.

In the coding of the above modifications, provision was made for either one or two burner lines. In addition, the position of the burner lines on the grid, as well as the number of grid points across which the heat and moisture are to be added, can be changed easily.

As opposed to the clear air comparisons with empirical temperature profiles that will be reported shortly, the sensitivity tests of Part II will involve an ambient fog. For these cases, a prescribed LWC is simply initialized at each grid point to the height desired.

h. Soil heat flux parameterization

During the course of the model investigations and comparison with empirical results, it was observed that an excess of heat existed at the surface in the numerical simulations. Assuming that heat loss to the soil is important, a simple parameterization of heat loss at the lower boundary of the model was developed.

It is assumed that sensible heat loss will occur at a rate determined by the difference in the air temperature T_a and a simulated ground temperature T_g, i.e.,

$$T_a^{t+1} = T_a^t \exp\left[\frac{-\delta(T_a^t - T_g)}{T_a^t}\Delta t\right], \quad (6)$$

where δ is a constant which determines the rate of heat loss by ground absorption. It is assumed that the soil is an infinite sink and thus that T_g remains unchanged, a realistic assumption for time periods on the order of minutes. The constant δ is defined such that it corresponds to the time required for one-half the temperature excess to be lost to the ground. For example, a δ defined for 1 min would mean that one-half the air temperature excess (over that of the ground) would be lost in 1 min. By varying this half-life, heat loss at the lower boundary can be adjusted to reproduce heat losses observed in empirical tests.

i. Addition of variable eddy coefficients

Murray's original model used K theory and constant eddy exchange coefficients to simulate subgrid-scale mixing. The use of variable or nonlinear eddy coefficients has provided one means of extending the applicability of K theory. Obviously, the degree of turbulent mixing, particularly under the buoyant conditions to be simulated in this study, is not constant in space. Neither can a constant coefficient be considered adequate in a model with a stretched grid.

In an effort to isolate an eddy viscosity parameterization which would yield the best results in this study, three separate parameterizations were coded into the model. These are discussed in detail in Tag *et al.* (1979) and are only outlined here.

The first parameterization is Smagorinsky's (1963) deformation formulation. In the two dimensions simulated here, it reduces to

$$K_M = (k_D\Delta)^2\left\{\left(\frac{\partial w}{\partial x} + \frac{\partial u}{\partial z}\right)^2 + 2\left[\left(\frac{\partial u}{\partial x}\right)^2 + \left(\frac{\partial w}{\partial z}\right)^2\right]\right\}^{1/2}, \quad (7)$$

where $\Delta = (\Delta x \Delta z)^{1/2}$ and k_D is a constant. Lilly (1967) showed that this formulation was consistent with the existence of an inertial subrange in three-dimensional (3D) turbulence and determined that a value of 0.2 for k_D was appropriate.

The second parameterization is based on the assumption that eddy viscosity does not depend on deformation alone, that stability must be included. Hill (1974), in his two-dimensional (2D) simulation of cumulus interactions, postulated that subgrid turbulence be linked to two time scales: one related to the deformation [as in Eq. (7)] and the other related to the buoyancy. He suggested that the buoyancy time scale be defined by the Brunt-Väisälä frequency, then summed the two components to yield

$$K_M = \Delta x \Delta z\left\{k_D^2\left[\left(\frac{\partial w}{\partial x} + \frac{\partial u}{\partial z}\right)^2 + 2\left(\left(\frac{\partial u}{\partial x}\right)^2 + \left(\frac{\partial w}{\partial z}\right)^2\right)\right]^{1/2} + k_B^2\left|\frac{g}{\bar{\theta}}\frac{\partial \theta}{\partial z}\right|^{1/2}\right\}, \quad (8)$$

where the buoyancy portion is set to zero if $\partial\theta/\partial z$ is positive.

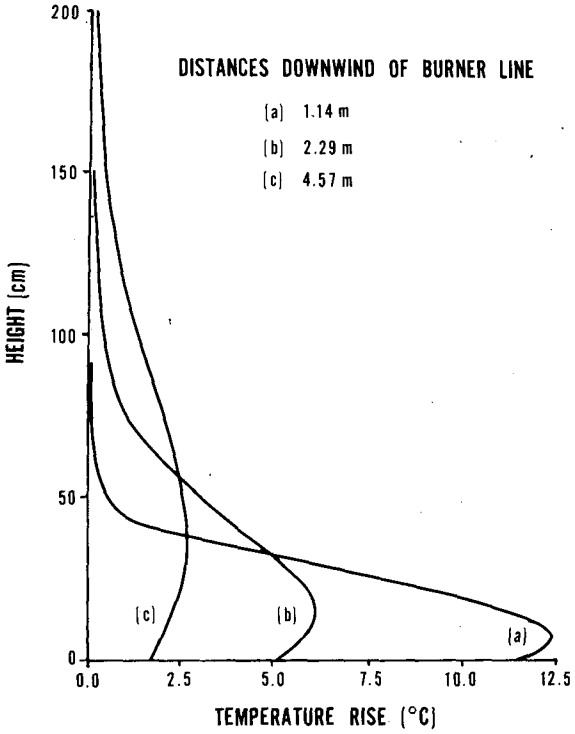

FIG. 2. Example of typical downwind temperature rise profiles derived from wind-tunnel experiments (from Rankine, 1950). The heat emission rate is 3.85×10^3 J m^{-1} s^{-1} and the cross-wind speed is 0.61 m s^{-1}.

The third parameterization is based on 2D turbulence theory. Although the situation simulated in this study, of course, is three-dimensional, the 2D forcing of a long burner line suggests that a 2D viscosity parameterization be considered. The concept of 2D turbulence was addressed by Kraichnan (1967) and again by Leith (1968). Of the two inertial ranges possible in 2D turbulence, Leith states that the -3 power law is the more logical form. Based on a constant enstrophy cascade, a 2D eddy viscosity coefficient can be formulated in a manner similar to that used in deriving (7):

$$K_M = (k_2\Delta)^3\left[\left(\frac{\partial\eta}{\partial x}\right)^2 + \left(\frac{\partial\eta}{\partial z}\right)^2\right]^{1/2}, \qquad (9)$$

where $\Delta = (\Delta x \Delta z)^{1/2}$ and k_2 is a dimensionless constant.

j. Eddy diffusivity

It is necessary that an assumption be made with regard to the ratio of K_T (or K_Q) to K_M. One common assumption is that they are equal; another is that the ratio is equal to 3. Based on analysis of fluctuating winds and temperatures from tower data, Businger *et al.* (1971) made estimates of this ratio. The trend for unstable conditions appeared clear and was approximated by

$$\frac{K_T}{K_M} = \frac{1.35(1 - 9\lambda)^{1/2}}{(1 - 15\lambda)^{1/4}}, \qquad (10)$$

where λ can be reasonably approximated by the Richardson number, more accurately as $\lambda \to -\infty$. Eq. (10) indicates that the ratio increases only linearly as $-\lambda$ increases logarithmically.

Several exploratory experiments were conducted using (10). Because areas of primary interest in the model domain are associated with moderate to extreme instability, Eq. (10) predicted ratios which were quite large. Such ratios, particularly where K_M is initially large itself, created difficulties in maintaining numerical stability using a reasonable time step. For this reason, a constant ratio of 3 was adopted for all runs. This value, according to Eq. (10), is accurate for moderate instabilities and not unreasonable for extreme instabilities.

3. Previous empirical studies

The technique of clearing fog by using heat was studied quite extensively during the World War II era. The primary effort, aside from burner design and other obvious considerations, went into subscale physical models which would predict temperature structures over burner lines situated under various ambient wind conditions. These results were then scaled upward in size to permit proper design of a full-scale installation. Although some work was conducted in the United States, more data, along with detailed explanations of the experimental layouts and apparatus, were provided by research conducted in England under Project FIDO. A detailed summary is given by Rankine (1950).

Measurements were taken in a specially constructed wind tunnel approximately 30 m long, 9 m wide and 3.5 m high. Air flow speeds and temperatures at several heights were measured. The position of a burner line, the amount of heat emitted by the line, and the speed of the wind in the tunnel were the primary controllable variables. Because of the difficulty of achieving consistent steady-state results, each experiment required on the order of 50 measurements at each instrumented site to produce a realistic average. The primary experimental arrangement was that of a single line situated in a cross wind. This case was considered to be the most important with regard to an operational system. Fig. 2, redrawn from Rankine's paper, illustrates the type of output derived from the experiments.

In addition to the wind tunnel scale, full-scale field experiments were conducted in order to verify the scaling laws (Froude number scaling) used to upscale the wind tunnel results. Two cases, differing both in heat output and wind speed, are presented in Rankine and are reproduced in Fig. 3. The full-scale measurements for these tests were made 69 m downwind of a 550 m burner line.

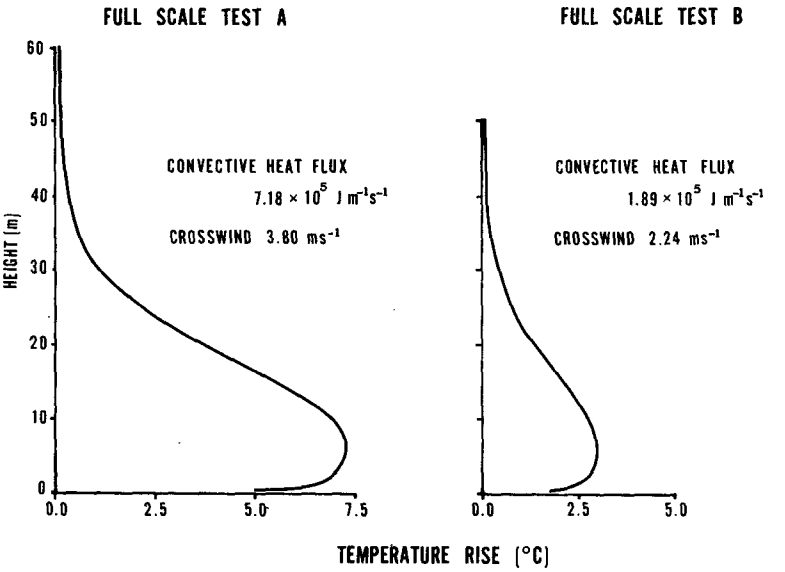

FIG. 3. Full-scale temperature rise profiles measured 69 m downwind of a 550 m burner line (from Rankine, 1950).

4. Model geometry and initial conditions

As noted in Section 3, data are available at two different scales: full and wind tunnel. Rather than scale the wind tunnel data upward for model comparison, it was decided to run the model at two separate scales. This course serves two purposes: first, it eliminates any need for (or required confidence in) direct scaling laws; and second, it permits a critical test of the model's inherent scaling, which must operate at scales one to two orders of magnitude apart. Fig. 4 is a schematic of the model geometry chosen for both scales for CRW experiments. After some experimenting, values of 0.5 for α and 0.1 for σ were chosen to prescribe the degree of stretching as defined by (1). Using these values, and setting the top of the domain at 500 m for full scale and 10 m for wind tunnel scale, maximum vertical resolution at the surface becomes 3 m and 6 cm, respectively. Based on Figs. 2 and 3 for typical experiments, the 500 and 10 m maximum heights appear to be well enough removed from the maximum heights of activity to cause little problem. As also depicted in Fig. 4, horizontal mesh resolutions of 10 m and 25 cm result in horizontal domains of 650 and 16.25 m, respectively. Again, Figs. 2 and 3 indicate that this choice permits sufficient horizontal resolution.

The primary input variables that specify the initial conditions for a typical run are 1) atmospheric sounding, 2) ambient wind speed, 3) heat release rate for burner line(s), 4) moisture release rate for burner line(s), 5) location of burner line within model domain and 6) liquid water content and depth of ambient fog.

The field data chosen for initial model testing are those of the two full-scale tests represented in Fig. 3. Initial conditions for full-scale tests A and B are given in Table 1.

Because temperature soundings were not given for these cases, an isothermal atmosphere of 7.5°C was chosen. The atmospheric sounding has little influence on the final distribution of heat, as will be shown later. The ambient wind is assumed constant with height and set at the measured values.

The rate of sensible heat release (for the model) is calculated to be 1.25 times the amount of heat measured 69 m downwind (from the empirical flux measurements) of the actual line—referred to as convective heat flux in Fig. 3. FIDO wind tunnel experiments revealed that ~20% of the combustible heat from the burning flames was lost to ground absorption and radiation; therefore, the rates of sensible heat addition specified in Fig. 3 are adjusted. Although moisture undoubtedly was emitted by the

TABLE 1. Initial conditions for full scale experiments.

Input parameters	Full-scale test A	Full-scale test B
Temperature/ dew-point sounding	isothermal, 7.5/6.5°C	isothermal, 7.5/6.5°C
Ambient wind	3.8 m s^{-1}	2.2 m s^{-1}
Heat input	8.975 × 10^5 J m^{-1} s^{-1}	2.364 × 10^5 J m^{-1} s^{-1}
Moisture input	none	none
Burner line location	surface, 60 m from upwind boundary	surface, 60 m from upwind boundary
LWC and depth of ambient fog	no fog	no fog

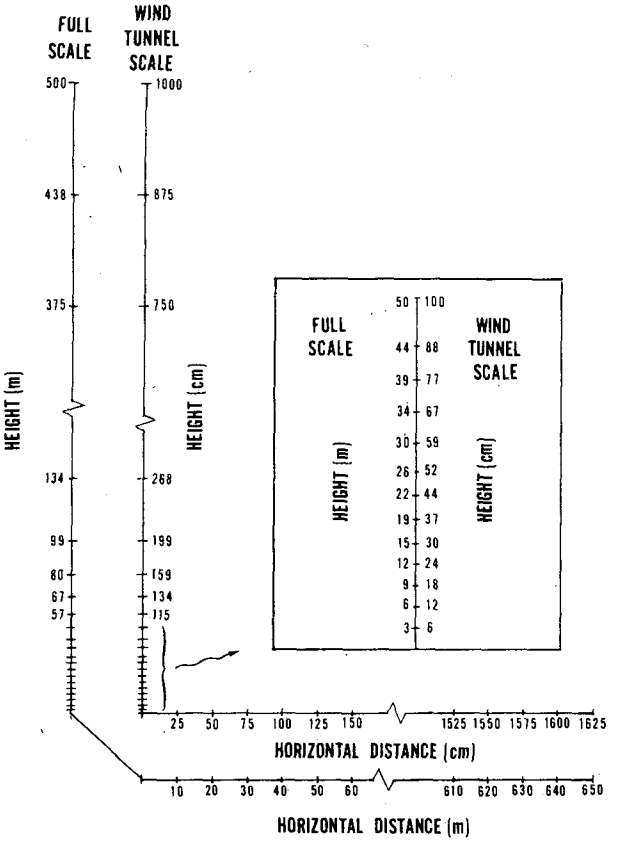

FIG. 4. Model domain for CRW experiments—horizontal and vertical resolution for both full and wind-tunnel scales.

hydrocarbon combustion, moisture release is omitted from these initial tests for simplicity. Exploratory experiments showed that the addition of moisture produces negligible differences for experiments conducted in clear air.

Because the area of interest in the model domain is downwind of the line, it is desirable to place the line as near to the upwind boundary as possible. However, allowance must be made for circulations upwind of the line to be properly simulated. A location 60 m downwind of the upwind (left) boundary was chosen as being satisfactory. And, because the lower boundary is rigid and no vertical velocity can exist there, no convection could arise if heat were input only at the lowest model grid point. For this reason, burner line releases are input at the lowest two grid points in the model domain.

And finally, because the full-scale experiments were performed in clear air, no ambient fog is initialized.

5. Comparison to observations—sensitivity test for K

a. Full scale

Using the initial conditions defined in Table 1, full-scale test A was chosen for the first observational comparisons. The purpose of these tests was to determine how well the model duplicates the measured temperature profiles, whether the choice of one variable eddy coefficient holds any advantage over the other, and whether the choice of the appropriate constants is critical.

The numerically predicted temperature profiles that follow are the approximate steady-state results 70 m downwind of the simulated line source of heat. These experiments were run for 3 min of simulated real time. Steady state, depending on distance down-

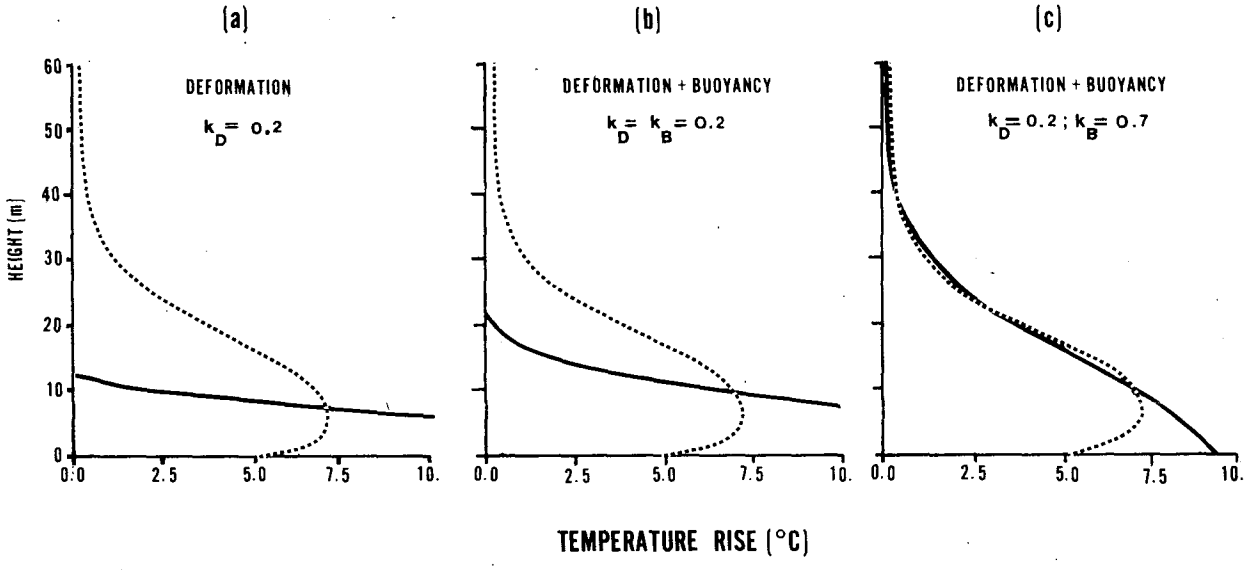

FIG. 5. A comparison of numerically predicted temperature rise profiles (solid lines) to observations (dashed lines) made in full-scale Test A (from Rankine, 1950) for three variations of eddy exchange coefficient. Initial conditions are outlined in Table 1.

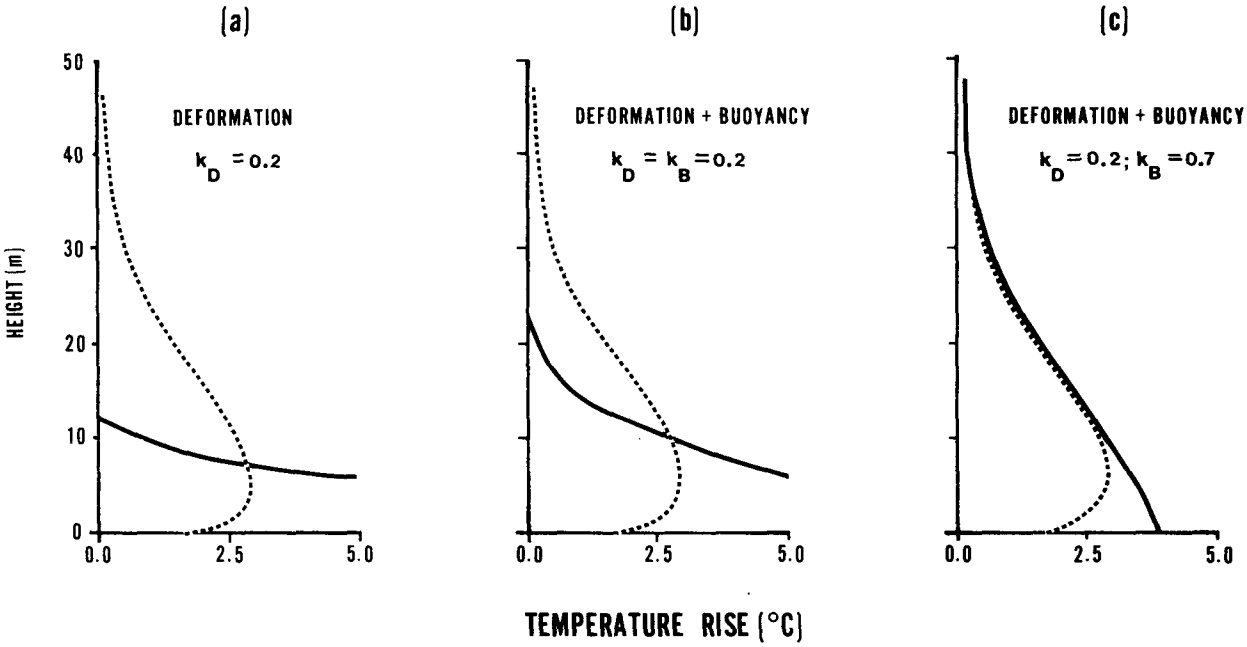

FIG. 6. As in Fig. 5 except for full-scale Test B. Initial conditions are outlined in Table 1.

wind and the wind speed, typically occurred after 2 min. Using a time step ranging from 0.25 to 0.50 s, the integrations took on the order of 5–10 min on a CDC CYBER 175.[5]

Smagorinsky's version (7) of the exchange coefficient, used here in its 2D form (neglecting terms involving v and gradients in y) and defining $\Delta = (\Delta x \Delta z)^{1/2}$, was tried first. Deardorff (1971) had determined that this formulation was adequate for weak thermal instability, using a value of 0.2 for the relevant constant k_D. The steady-state temperature profile using this formulation for test A is plotted alongside the empirical curve in Fig. 5a. The comparison is quite surprising; the model prediction is very poor. Whereas a temperature excess is measured well above 30 m in the field experiment, the same excess barely reaches 12 m in the model experiment. As a result, the heat is unrealistically concentrated near the ground in a shallow layer.

Because the next logical step in attempting a realistic numerical simulation appeared to be to include a buoyancy-dependent term, as Hill had done, the combined deformation-buoyancy form (8) was tried next. An appropriate first step was to assume that the buoyancy-related constant k_B might possibly also be equal to 0.2. The resulting comparison, given in Fig. 5b, shows only slight improvement over Fig. 5a.

In his cumulus interaction studies, Hill (1974) experimented with several different values of k_D and k_B, both being equal in his model. He conducted four experiments in which k_D and k_B varied from approximately 0.22 to 0.63, with two values in between. The four were then compared with regard to cloud-top height, cloud diameter and growth rate. Comparisons with observations were also made. The cloud growth rate was found to be the most sensitive to changes in k_D and k_B. The value which gave the best results for growth rates, when compared to observations, was the largest value, 0.63.

Consequently, k_B was increased to determine if comparisons with field results would improve. (Because of Lilly's determination that 0.2 is the appropriate constant for a K_M based on the deformation, k_D was left unchanged at 0.2.) Consistent with Hill's findings, the comparisons improved. The best results were found with a value of 0.7 for k_B and are shown in Fig. 5c. The comparison is much better than either Fig. 5a or 5b. Heat is mixed sufficiently high to produce agreement at the highest levels of observation. It will be noted that the predicted profile is not in agreement near the surface; this was expected, since the soil heat flux parameterization was not included. Because, in terms of clearing fog, there is more than enough heat near the surface, no attempt will be made to produce agreement until the soil heat flux parameterization is included later in this study.

Having produced good agreement with full-scale test A, it remained to be determined whether the critical value found for k_B would produce equally good results for test B. As summarized in Table 1, cases A and B are quite different. The cross-wind

[5] For this particular model, the CYBER 175 is approximately seven times faster than a CDC 6500.

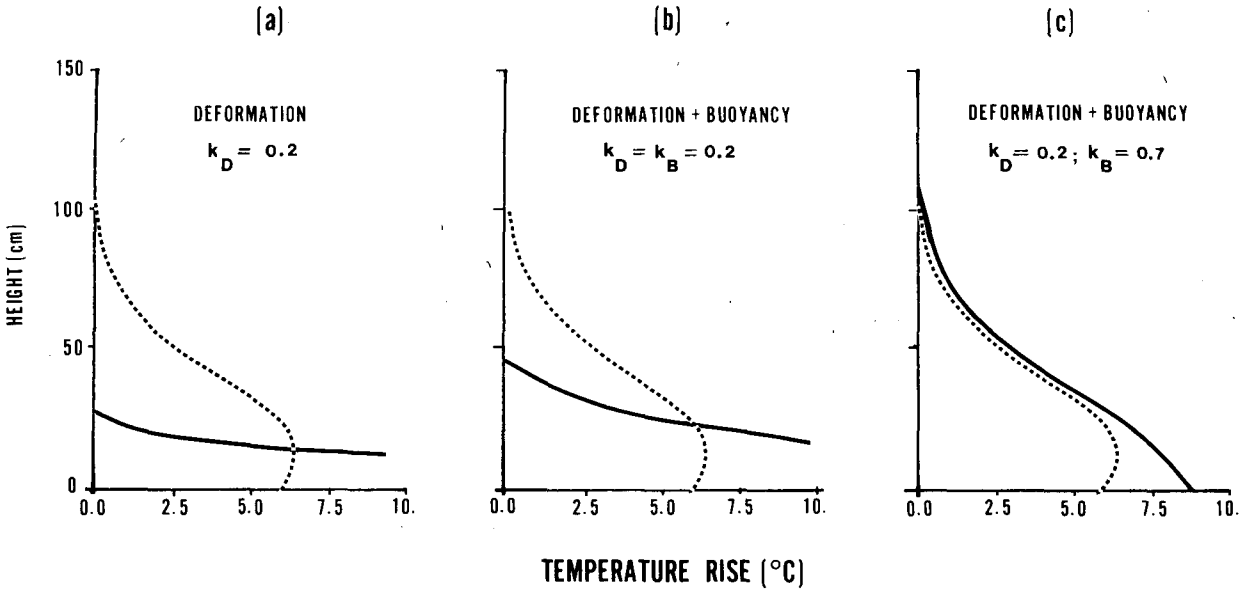

FIG. 7. A comparison of predicted temperature rise profiles (solid) to observations (dashed) made in a wind tunnel (from Rankine, 1950) for three variations of eddy exchange coefficient. The heat emission rate is 3.85×10^3 J m^{-1} s^{-1} and the cross-wind speed 0.73 m s^{-1}.

speed of test B is 60%, while the heat emitted from the line is only 25%, of that for test A. Fig. 6 summarizes the same three coefficient variations (as in Fig. 5) for this second case. The relative comparisons between Figs. 5 and 6 are nearly identical, with the same good agreement for $k_B = 0.7$.

The steady-state comparisons depicted in Figs. 5 and 6 obviously are the culminating results from dozens of integrations. During this testing, many combinations of eddy coefficient form and appropriate constants were tried. From a comparison of the individual plots, it is clear that the buoyancy parameterization is more important than the wind shear parameterization. Use of the 2D eddy coefficient (9), with a value for k_2 of 0.2, in combination with the buoyancy term, gave nearly identical results to that shown in either Fig. 5c or 6c. A value for k_2 as large as 0.7 failed to give realistic results for the 2D form when used alone with no buoyancy addition. Thus it would appear that for the strongly buoyant conditions studied in this report, eddy coefficients must be buoyancy dependent and a numerical simulation based solely on vorticity gradients or the deformation is not adequate.

b. Subscale

Having determined a form of coefficient (and its constants) which produces satisfactory results for field scale experiments, comparisons with wind tunnel tests (for which there are more data) were initiated. A second successful simulation at this much smaller scale would result from the fulfillment of two assumptions. One is that the same physical processes active at large scale are likewise active at wind-tunnel scale. And second, it must be assumed that the eddy coefficient, which is linked not only to wind shear and buoyancy but also to the scaling manifest in the grid size chosen for the model domain, maintains its integrity through almost two orders of magnitude grid-size reduction.

The grid spacing and related stretching for the small-scale experiments were shown in Fig. 4. The smaller scale of simulations enabled steady-state results to be obtained in a shorter time (typically 20–30 s), but also required the time steps to be reduced significantly—ranging from 0.015 to 0.030 s.

Rankine's measurements were made at three distances downwind of the wind tunnel burner line: 1.14, 2.28 and 4.57 m. For these first comparisons, the mid-distance temperature profile was used. An experiment in which the heat release rate was 3.85×10^3 J m^{-1} s^{-1} and the cross wind 0.91 m s^{-1} was chosen for the first comparison. No adjustment to the heat release rate, as was made for full scale, was necessary since the reported rate was that of combustible heat released directly at the line, rather than that calculated by flux measurements downwind. However, the specified cross wind was that measured at the top of the wind tunnel (1.52 m) and was slightly larger than that found nearer the floor. An analysis of the wind speed distribution with height, under conditions with no burner line operating, indicated that a value ~80% of the quoted wind speed would be more typical of conditions in the first 25–50 cm above the floor of the tunnel.

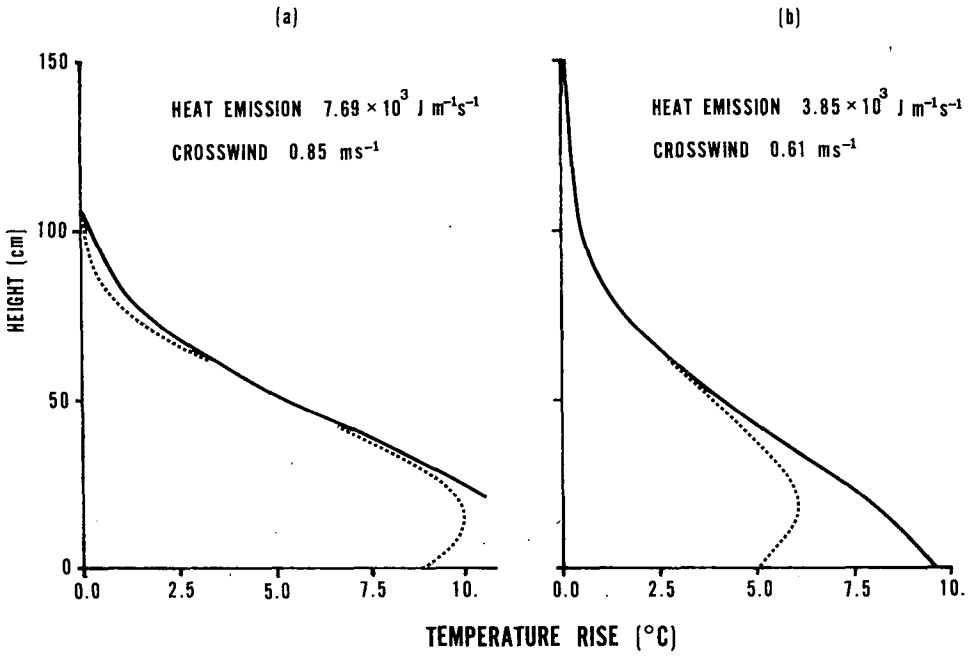

FIG. 8. As in Fig. 7 except for two additional wind-tunnel experiments. The eddy exchange formulation is the same as that used in Figs. 5c, 6c and 7c.

The same sequence as shown in Figs. 5 and 6 is given in Fig. 7 for the experiment described above. The same poor agreement results for the deformation form and the one combined form, while Fig. 7c reveals the same good agreement as found for the full-scale tests. This result proved quite encouraging. Two additional cases for other values of heat release and wind speed were simulated (results are shown in Fig. 8) and again the agreement is good.

The next required test was a comparison at the two other downwind observation points. Rankine plotted data for the experiment represented in Fig. 8b: a heat release rate of 3.85×10^3 J m^{-1} s^{-1} in a cross flow of 0.61 m s^{-1}. The numerical profiles were plotted alongside this data (Fig. 9) for the downwind distances 1.14 and 4.57 m. Obviously, although the agreement is not poor, it is not nearly as good as it was for the mid-range comparison. Heat is mixed too high near the source of heat (Fig. 9a) but not quite high enough farther downwind (Fig. 9b). Comparisons for other cases revealed the same tendency.

In an attempt to produce better agreement at these two additional downwind locations, a closer examination of the coefficient parameterizations and their related constants was made. Other combinations were tried. A comparison of Figs. 9a and 9b clearly shows that no manipulation of k_B alone will produce better agreement; because the difference between the empirical and numerical results is reversed, any change in k_B will merely accentuate the error at one end or the other. Another variation was tried: the earlier established dictum that k_D must remain unchanged at 0.2 was temporarily dropped. For example, Hill's assumption that k_D and k_B are equal was tried. No better agreement was found using various constants. Another alternative was to weight deformation more heavily than buoyancy. This option provided worse results. Use of the 2D form, either alone or in combination with buoyancy, produced poor comparisons with all variations of constants. Use of a constant eddy coefficient also proved fruitless. Numerous integrations revealed that no better comparisons (than those in Figs. 8b, 9a and 9b) could be effected by any of the above options. Because the overall comparison for the combined form (and the determined constants) proved reasonably accurate, it was chosen for subsequent experiments.

Rankine provided wind speed measurements at various heights in the wind tunnel, in addition to the temperature profiles. Data were taken both with the burner lines turned on and off. Differences between these two values (both empirical and numerical) as a function of height are plotted in Fig. 10. Comparisons for the three downwind locations are given for the same experiment depicted in Figs. 8b and 9. Points are plotted to the maximum height given by Rankine. Both empirical and numerical results reveal that wind speed is enhanced by heating from the line source. Second, the maximum increase occurs near the surface and decreases with height. Agreement between the observations and the numerical results is reasonable, with the absolute dif-

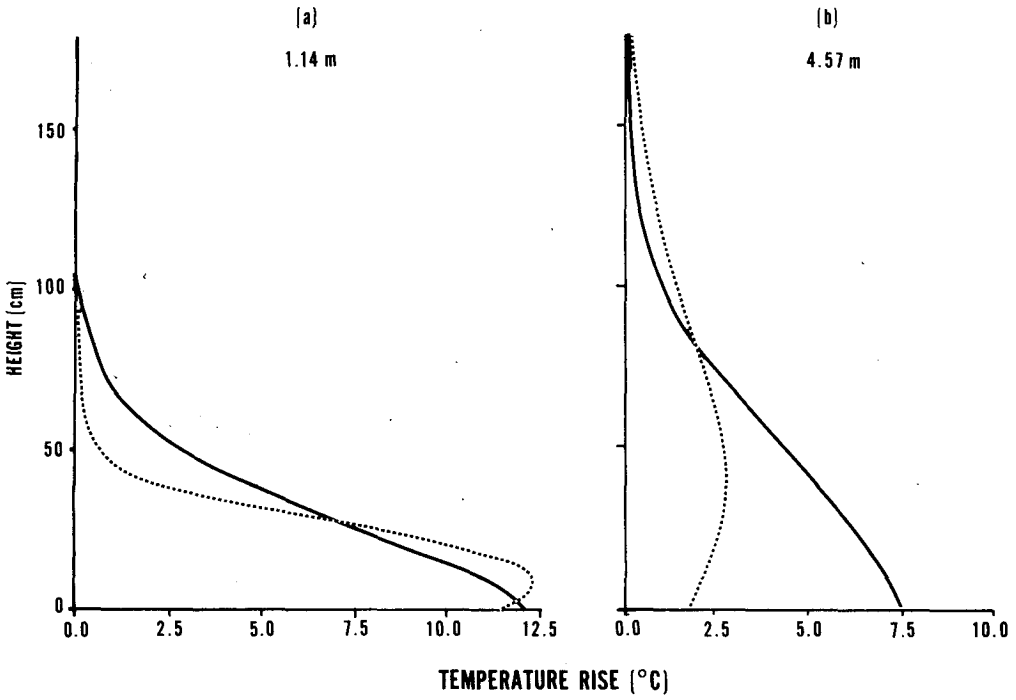

FIG. 9. A comparison of predicted temperature rise profiles (solid) to observations (dashed) made at two additional downwind distances for the same experiment depicted in Fig. 8b: heat release of 3.85×10^3 J m^{-1} s^{-1}; cross flow of 0.61 m s^{-1}.

ferences of the numerical consistently lower than those of the empirical. Discussion of these wind speed increases will be expanded later in Part II.

6. Soil heat flux parameterization

As evident from all of the empirical temperature traces used for comparison, the maximum temperature at a distance downwind from the burner line occurs slightly above the surface rather than at the surface. For the numerically predicted profiles, however, the maximum always occurs at the surface. Rankine concluded that the blunted "nose" of the profile resulted from heat loss to the ground or floor of the wind tunnel. Attempting to duplicate this effect led to the soil heat flux parameterization, which is only a crude tool used to try to duplicate the observed results. A better approach would be to prescribe a heat balance equation at the lower boundary.

Because energy creation and losses were more accurately determined in the wind tunnel, a wind-tunnel experiment was used for the following tests. Based on heat flux measurements and the calorific content of the fuel, Rankine calculated that 20% of the heat released was lost downwind of the burner line. It was estimated that one-quarter was due to floor absorption and the remainder to radiation losses. Moreover, it was determined that most of this heat loss occurred closer to the line than the first observational point (1.14 m). The excess energy (represented, approximately, by the area between the empirical and numerical curves) in Figs. 7c and 8 supports the general magnitude of Rankine's estimate of heat loss. For example, in Fig. 7c, approximately 15% of the initial empirical energy has been lost.[6] For the experiment represented in Fig. 8b, the amount is about 18%. These results also suggest that Rankine's calculations of the calorific heat emitted at the line were fairly accurate, since no assumption need be made in the model regarding combustion efficiencies; heat input and energy conservation are known exactly.

The purpose of the following numerical simulations is to determine if a 5% loss of sensible heat to the floor is enough to cause the maximum temperature to be elevated off the floor. The remaining 15% radiational heat loss will not be numerically simulated; consequently, excess heat will still exist in the numerical profiles. The experiment in which the 20% heat loss estimate of Rankine proved to be very accurate (Fig. 8b—3.85×10^3 J m^{-1} s^{-1}; 0.61 m s^{-1}) was chosen for testing.

As described earlier, the heat flux parameterization requires two input parameters. One is the floor temperature, which remains unchanged, and the

[6] The "lost" energy is approximated to be the area under the numerical curve minus the area under the empirical curve, all divided by the former.

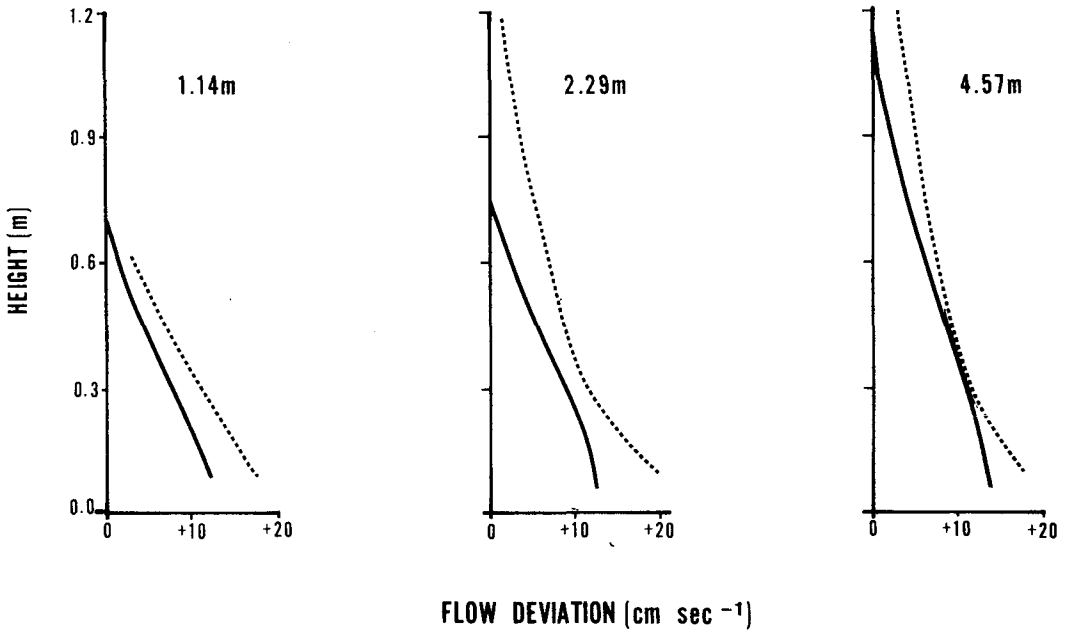

FIG. 10. Deviation of heated flow from nonheated ambient flow as a function of height for experiment depicted in Fig. 8b and 9. Solid lines, numerical; dashed lines, empirical.

second is the constant which prescribes the rate of heat withdrawal. As an arbitrary estimate of the floor temperature (since no such data was presented by Rankine), it was assumed to be 5 K colder than the ambient air of 280.66 K. Several values of the relevant constant were tried and the resultant heat loss (as a percentage of the total) calculated for each case.

The results for three experiments that bridge the 5% loss estimated by Rankine are given in Figs. 11b, 11c, and 11d. They can be compared to Fig. 11a (a duplicate of Fig. 8b) which assumes no surface heat loss. This comparison reveals that a 5% loss of heat is adequate for elevating the maximum temperature to a point above the surface. As shown in Fig. 11d, the "nose" can be elevated slightly higher if more heat is removed. Rankine's estimate of 5% heat loss to the floor may have been low. The point illustrated by this exercise, however, is that a 5% heat loss can explain the elevated maximum tem-

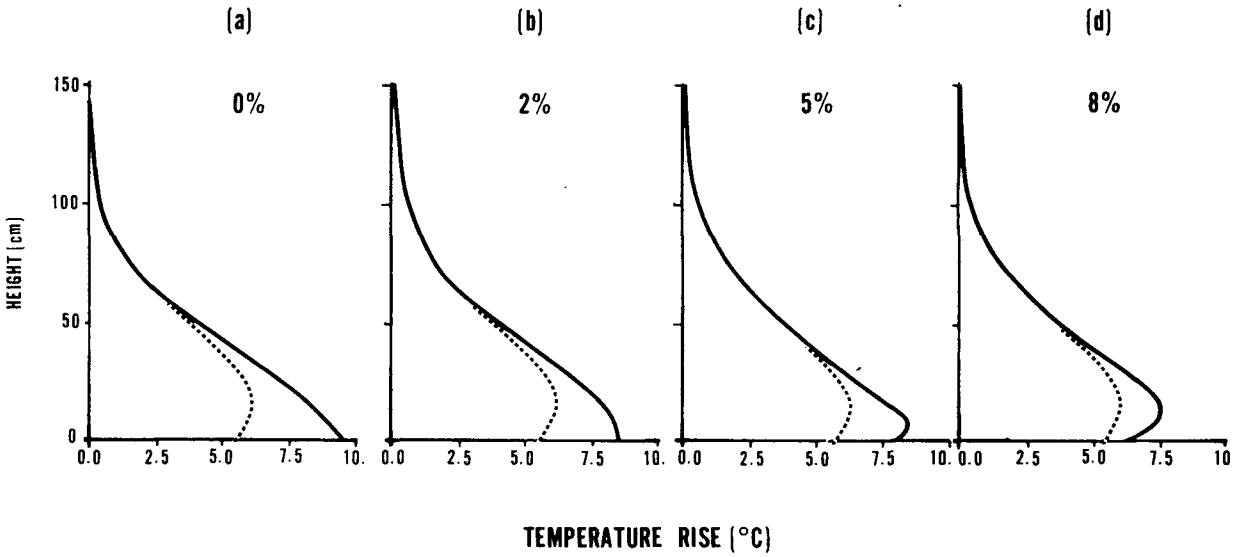

FIG. 11. Steady-state temperature profiles resulting from several different rates of surface heat loss: (a) no soil heat loss; (b), (c), (d) increasing heat removal resulting in the specified percentage of total heat loss.

peratures observed both in the wind-tunnel and outdoor experiments. In terms of fog dissipation, this point is purely academic since there is more than enough heat available at the surface.

7. Summary and conclusions

A two-dimensional model intended for simulating the dissipation of fog using passive burner lines has been developed and model results compared to data collected from burner lines operating both outdoors and in a wind tunnel.

Much of the model development effort was spent finding a form of variable eddy coefficient which could provide satisfactory comparisons with the observed data. It was determined that a coefficient based solely on the deformation or vorticity gradients was inadequate, and that a buoyancy-dependent form was necessary. A form in which the deformation and buoyancy effects were summed, with the latter weighted more heavily, gave good results. Equally good comparisons were achieved with two different sets of full-scale data. Data taken from wind-tunnel experiments, for which the model domain was reduced in size by two orders of magnitude, were used to further test the eddy viscosity parameterization. In contrast to the outdoor measurements, wind-tunnel observations were made at three separate downwind locations. The middle location produced as good a comparison as had been achieved for full scale. This result implied that the same physical processes active at full scale are likewise active at wind-tunnel scale. It also demonstrated that the eddy viscosity, which is a function of the grid spacing, could maintain its integrity through almost two orders of magnitude reduction in grid size. Observational data from the two alternate downwind locations resulted in slightly poorer but still acceptable comparisons. Additional wind-tunnel comparisons involving wind speed data produced good general agreement. A final set of experiments utilizing the soil heat flux parameterization supported empirical estimates of a 5% heat loss to the soil.

The use of the model to investigate fog dissipation under varying atmospheric conditions and different burner line positionings will be explored in Part II of this paper.

Acknowledgments. Research for this paper was conducted at the Naval Environmental Prediction Research Facility where over a period of 3½ years, Commanding Officers Captains Glenn D. Hamilton, Robert C. Sherar, and Pierre A. Petit all offered encouragement and support. This paper also formed the core of a Ph.D. dissertation at the Pennsylvania State University.

Special thanks are due Dr. John D. Lee, who provided valuable guidance and assistance during the entire course of this research.

Several others are due grateful acknowledgment. Mr. Paul R. Lowe, the author's supervisor during most of this work, originally suggested and supported this research. In addition, he provided valuable guidance in the use of the Murray cumulus model. Dean Charles L. Hosler and Dr. Bernard A. Silverman offered encouragement. Several discussions with Drs. Yoshi K. Sasaki and Thomas E. Rosmond were most helpful. Appreciation is also due Dr. Rosmond for his assistance in implementing the fast Poisson solver. Dr. Alan I. Weinstein and Mr. Bruce A. Kunkel provided both data and useful guidance based on the U.S. Air Force warm fog dispersal program. And finally, I wish to thank Ms. Winona Carlisle for typing the manuscript and AG1 James Carlson for drafting the figures.

REFERENCES

Businger, J. A., J. C. Wyngaard, Y. Izumi and E. F. Bradley, 1971: Flux profile relationships in the atmospheric surface layer. *J. Atmos. Sci.*, **28**, 181–189.

Deardorff, J. W., 1971: On the magnitude of the subgrid scale eddy coefficient. *J. Comput. Phys.*, **7**, 120–133.

Hill, G. E., 1974: Factors controlling the size and spacing of cumulus clouds as revealed by numerical experiments. *J. Atmos. Sci.*, **31**, 646–673.

Kraichnan, R. H. 1967: Inertial ranges in two-dimensional turbulence. *Phys. Fluids*, **10**, 1417–1423.

Kunkel, B. A., 1979: A modern thermo-kinetic warm fog dispersal system for commercial airports. *J. Appl. Meteor.*, **18**, 794–803.

——, B. A. Silverman and A. I. Weinstein, 1974: An evaluation of some thermal fog dispersal experiments. *J. Appl. Meteor.*, **13**, 666–675.

Leith, C. E., 1968: Diffusion approximation for two-dimensional turbulence. *Phys. Fluids*, **11**, 671–673.

Lilly, D. K., 1967: The representation of small-scale turbulence in numerical simulation experiments. *Proc. IBM Scientific Computing Symp. Environmental Sciences*, IBM Data Processing Div., White Plains, NY, 195–210.

Murray, F. W., 1970: Numerical models of a tropical cumulus cloud with bilateral and axial symmetry. *Mon. Wea. Rev.*, **98**, 14–28.

——, and L. R. Koenig, 1972: Numerical experiments on the relation between microphysics and dynamics in cumulus convection. *Mon. Wea. Rev.*, **100**, 717–732.

Rankine, A. O., 1950: Experimental studies in thermal convection. *Proc. Phys. Soc.*, **B63**, 225–251.

Roach, P. J., 1972: *Computational Fluid Dynamics*. Hermosa Publishers, 434 pp.

Rosmond, T. E., and F. D. Faulkner, 1976: Direct solution of elliptic equations by block cyclic reduction and factorization. *Mon. Wea. Rev.*, **104**, 641–649.

Smagorinsky, J. S., 1963: General circulation experiments with the primitive equations: I. The basic experiment. *Mon. Wea. Rev.*, **91**, 99–164.

Tag, P. M., 1977: A numerical simulation of warm fog dissipation by electrically enhanced coalescence: Part II. Charged drop seeding. *J. Appl. Meteor.*, **16**, 683–696.

——, F. W. Murray and L. R. Koenig, 1979: A comparison of several forms of eddy viscosity parameterization in a two-dimensional cloud model. *J. Appl. Meteor.*, **18**, 1429–1441.